IL NUOVO CIMENTO **42 C** (2019) 250
DOI 10.1393/ncc/i2019-19250-3

COLLOQUIA: La Thuile 2019

CP violation in charm at LHCb

T. PAJERO[1][2] on behalf of the LHCb COLLABORATION

([1]) *Scuola Normale Superiore - Pisa, Italy*
([2]) *INFN, Sezione di Pisa - Pisa, Italy*

received 10 October 2019

Summary. — While the CKM paradigm of CP violation has been tested extensively in K and B mesons, CP violation remains unobserved in the decay of up-type quarks. The study of CP violation in charm decays is thus a complementary test of the Standard Model, since it allows constraining CP-violating operators that might leave the observables of down-type quarks unaffected. Two recent measurements of CP violation in charm decays by the LHCb Collaboration are reviewed. Their precision, below the 10^{-3} level, is finally entering the upper limit of the range of Standard Model predictions. The forthcoming Upgrade I of LHCb (2021–2029) will allow pushing the precision of the searches for CP violation in charm below the 10^{-4} level.

1. – Introduction

In the Standard Model (SM) of particle physics, violation of charge-parity (CP) symmetry originates from a single complex phase in the Cabibbo–Kobayashi–Maskawa (CKM) matrix [1]. While the CKM paradigm for CP violation (CPV) is experimentally well established in the K- and B-meson systems, additional sources of CPV are required to explain the cosmological observations of the relative abundance of matter and antimatter in the Universe [2]. The charm quark is the only up-type quark forming bound states for which CPV can be measured. In the SM, the greatest CP asymmetries are expected in the time-integrated asymmetries of Cabibbo-suppressed (CS) $c \to d\bar{d}u$ and $c \to s\bar{s}u$ decays and originate from the interference of tree- and loop-level amplitudes. Owing to the smallness of the elements of the CKM matrix involved and to the Glashow–Iliopoulos–Maiani suppression mechanism, they are predicted to be of the order of 10^{-4} to 10^{-3} [3], with nonnegligible uncertainties due to low-energy QCD effects. However, they might be enhanced by interactions beyond the SM, such as QCD penguin and chromomagnetic dipole operators [3], which, again, would mainly affect CS decay amplitudes, while leaving the CPV observables of down-type quarks unaffected [3].

The huge data samples needed to test the SM expectations for CPV in charm, order of 10^7 decays, have become available only recently thanks to the large $c\,\bar{c}$ production

cross-section at the LHC [4] and to the dedicated detector and trigger of the LHCb experiment [5]. This is a single-arm forward spectrometer covering the pseudorapidity range $2 < \eta < 5$, designed for the study of particles containing b or c quarks. Particularly important for the measurement of charm decays is the silicon-strip vertex detector surrounding the $p\,p$ interaction region, which provides an uncertainty on the measurement of the impact parameter of the tracks of $(15 + 29/p_{\mathrm{T}})\,\mu\mathrm{m}$, where the transverse momentum is measured in GeV/c, and allows to identify c hadrons from their typically long flight distance (order of 1 cm). Particle identification of pions and kaons, which is provided by two ring-imaging Čerenkov detectors, reduces drastically the contamination of the signal samples from backgrounds of partially reconstructed and misidentified decays of c hadrons. Finally, an essential feature is the high trigger output rate, about 12 kHz, which is allowed by the Turbo data-taking paradigm adopted since 2015 [6]. This provides events reconstruction with offline-like quality already at the trigger level and allows performing physics analyses directly on the candidates reconstructed in the trigger. The storage of only the triggered candidates enables a reduction in the event size by an order of magnitude.

This document is organised as follows: two recent measurements of *CPV* in the decay are presented in sects. **2** and **3**. Section **4** concludes commenting on the prospects for charm *CPV* measurements at LHCb in the next few years.

2. – Search for *CP* violation in $D_s^+ \to K_{\mathrm{S}}^0\pi^+$, $D^+ \to K_{\mathrm{S}}^0K^+$ and $D^+ \to \phi\pi^+$ decays

Two-body decays of charm mesons into charged hadrons (or into particles decaying into charged hadrons like the ϕ meson or the K_{S}^0 meson) are good candidates for the discovery of *CPV* in the charm sector at the LHCb experiment, since they are reconstructed with relatively high efficiency thanks to its excellent tracking system and to the average high momentum and low multiplicity of the particles in the final state. As a consequence, yields of order of 10^7 are obtained in many CS decay channels, attaining precisions on *CP* asymmetries below the 10^{-3} level.

A recent search measures the *CP* asymmetry of the CS decay rates of $D_s^+ \to K_{\mathrm{S}}^0\pi^+$, $D^+ \to K_{\mathrm{S}}^0K^+$ and $D^+ \to \phi\pi^+$ decays([1]) employing the data collected during 2015–2017, corresponding to 3.8 fb^{-1} of integrated luminosity of $p\,p$ collisions at $\sqrt{s} = 13$ TeV [7]. The K_{S}^0 (ϕ) mesons are reconstructed using the $\pi^+\pi^-$ (K^+K^-) decay channel. The ϕ-meson reconstructed invariant mass is required to be within $10\,\mathrm{MeV}/c^2$ from its known value [8], while possible contributions from interfering decay amplitudes in the $D^+ \to K^+K^-\pi^+$ Dalitz plot are neglected. The raw asymmetry, defined as the asymmetry between the signal yields of $D_{(s)}^+$ and $D_{(s)}^-$ decays, can be written as

$$\mathcal{A}_{\mathrm{raw}}(D_{(s)}^+ \to f^+) \approx \mathcal{A}_{CP}(D_{(s)}^+ \to f^+) + \mathcal{A}_{\mathrm{P}}(D_{(s)}^+) + \mathcal{A}_{\mathrm{D}}(f^+), \tag{1}$$

where the first term on the right-hand side is the *CP* asymmetry in the decay, the second is the production asymmetry of $D_{(s)}^+$ mesons, the third is the detection asymmetry of the final state due to different reconstruction efficiencies of positively and negatively charged particles and of K^0 and $\overline{K}^0$ mesons, and terms of order three or higher in the asymmetries are neglected. The production and detection asymmetries are cancelled

([1]) The inclusion of charge-conjugate processes is implied throughout.

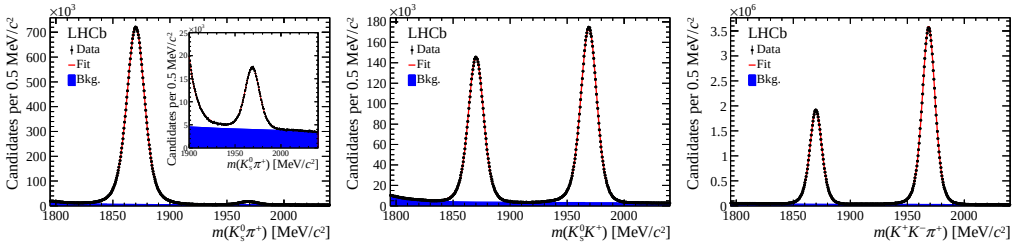

Fig. 1. – Mass distribution of the selected (left) $D^+_{(s)} \to K^0_S\pi^+$, (middle) $D^+_{(s)} \to K^0_S K^+$ and (right) $D^+_{(s)} \to \phi\pi^+$ candidates with fit projections overlaid. The inset in the left plot shows the mass distribution around the $D^+_s \to K^0_S\pi^+$ signal region.

using the Cabibbo-favoured (CF) control samples $D^+ \to K^0_S\pi^+$, $D^+_s \to K^0_S K^+$ and $D^+_s \to \phi\pi^+$, for which the *CP* asymmetry is negligible with respect to CS decays in the SM and also in most models beyond the SM, since $c \to s\bar{d}u$ transitions are unaffected by QCD penguin and chromomagnetic dipole operators. In particular, the *CP* asymmetries of the CS decays are determined as

$$\mathcal{A}_{CP}(D^+_s \to K^0_S\pi^+) \approx \mathcal{A}_{\rm raw}(D^+_s \to K^0_S\pi^+) - \mathcal{A}_{\rm raw}(D^+_s \to \phi\pi^+), \tag{2a}$$

$$\begin{aligned}\mathcal{A}_{CP}(D^+ \to K^0_S K^+) \approx\ & \mathcal{A}_{\rm raw}(D^+ \to K^0_S K^+) - \mathcal{A}_{\rm raw}(D^+ \to K^0_S\pi^+) \\ & - \mathcal{A}_{\rm raw}(D^+_s \to K^0_S K^+) + \mathcal{A}_{\rm raw}(D^+_s \to \phi\pi^+),\end{aligned} \tag{2b}$$

$$\mathcal{A}_{CP}(D^+ \to \phi\pi^+) \approx \mathcal{A}_{\rm raw}(D^+ \to \phi\pi^+) - \mathcal{A}_{\rm raw}(D^+ \to K^0_S\pi^+), \tag{2c}$$

where the contribution from the K^0 detection asymmetry is omitted but is subtracted where relevant following the procedure described in ref. [9], which takes into account the material distribution of the LHCb detector, the different cross-section with matter of K^0 and $\overline{K}^0$ mesons and the known *CPV* in the time evolution of K^0 mesons [10]. Only K^0_S candidates that decayed within the vertex detector are considered to make $D^+_{(s)} \to K^0_S h^+$ candidates, in order to reduce to a negligible level the *CPV* arising from the interference of Cabibbo-favoured and doubly Cabibbo-suppressed amplitudes with the kaon-meson mixing in the CF samples [10]. Since both the production and the detection asymmetries depend on the kinematics of the relevant particles, the kinematics of the $D^+_{(s)}$ meson and of the charged hadron responsible of the detection asymmetry of the CF samples are weighted to those of the corresponding particles of the CS sample before measuring the asymmetries.

The asymmetries are determined through a simultaneous least-squares fit of the mass distributions of positively and negatively charged $D^+_{(s)}$ mesons. In each fit, the signal component is modelled as the sum of a Gaussian function and a Johnson S_U function [11], which accounts for asymmetric tails, whereas the combinatorial background is described by the sum of two exponential functions. The mass distributions with the fit projections are displayed in fig. 1. The samples contain approximately 0.6 million $D^+_s \to K^0_S\pi^+$, 5.1 million $D^+ \to K^0_S K^+$ and 53.3 million $D^+ \to \phi\pi^+$ CS candidates and 30.5 million $D^+ \to K^0_S\pi^+$, 6.5 million $D^+_s \to K^0_S K^+$ and 107 million $D^+_s \to \phi\pi^+$ CF candidates.

The dominant systematic uncertainty for all decay modes is due to the assumed shapes in the fits to the mass distribution. This is evaluated by fitting with the nominal model large sets of pseudoexperiments generated with alternative models that describe data equally well. For the $D^+ \to \phi\pi^+$ decay mode, a systematic uncertainty of 0.15×10^{-3} arises from neglected kinematic differences between the ϕ-meson decay products (see

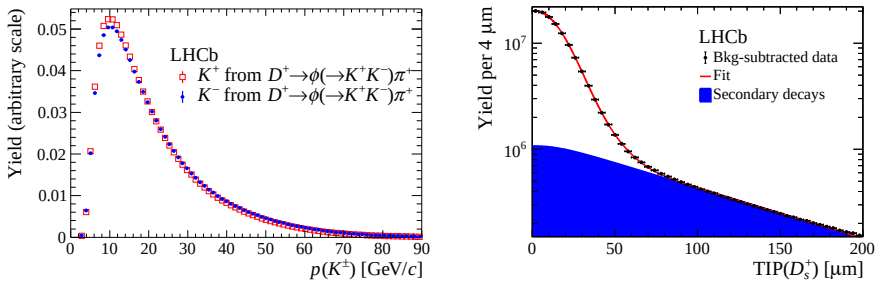

Fig. 2. – (Left) Comparison between background-subtracted normalised distributions of the kaon momenta the for the $D^+ \to \phi\pi^+$ sample. (Right) Distribution of the transverse impact parameter for background-subtracted $D_s^+ \to K_S^0\pi^+$ candidates with fit projections overlaid.

fig. 2 left). These differences are mainly caused by the interference between the S-wave and the $\phi\pi^+$ decay amplitudes and result into an imperfect cancellation of the detection asymmetry of K^+ and K^- mesons, even if the K^+K^- final state is self conjugate. For the other decay modes, the second leading systematic uncertainty is due to the signal contamination from secondary $D_{(s)}^+$ decays, where the $D_{(s)}^+$ meson is produced in the decay of a b hadron instead of in the p p collision. The size of this background is estimated through fits to the $D_{(s)}^+$-meson impact parameter in the plane transverse to the beam (fig. 2 right). Its fraction is slightly different for CS and CF decays, resulting into slightly different production asymmetries for CS and CF candidates. Finally, subleading contributions arise due to small kinematic differences between the CS and CF samples that are not completely removed by the kinematic weighting, and to the finite precision of the subtraction of the neutral-kaon detection asymmetry.

The results, which are all consistent with the hypothesis of no CP violation, are

$$\mathcal{A}_{CP}(D_s^+ \to K_S^0\pi^+) = (\ \ 1.3\ \ \pm 1.9\ \ \pm 0.5\ \ ) \times 10^{-3}, \tag{3a}$$

$$\mathcal{A}_{CP}(D^+ \to K_S^0 K^+) = (-0.09 \pm 0.65 \pm 0.48) \times 10^{-3}, \tag{3b}$$

$$\mathcal{A}_{CP}(D^+ \to \phi\pi^+) = (\ \ 0.05 \pm 0.42 \pm 0.29) \times 10^{-3}, \tag{3c}$$

where the first uncertainties are statistical and the second systematic. This is the most precise determination of these quantities to date and, more generally, the most precise measurements of CPV in the decay in the charm sector at the time that this conference took place.

3. – Search for CP violation through an amplitude analysis of $D^0 \to K^+K^-\pi^+\pi^-$ decays

Multibody D^0-meson decays are interesting decay channels to look for CPV. In fact, they have a rich resonant structure, and the variation of the QCD strong phases across the multidimensional phase space of the final state may provide regions with enhanced sensitivity to CPV. In addition, amplitude analyses of $D^0 \to K^+K^-\pi^+\pi^-$ decays are important as possible measurements of the CKM angle γ with $B^- \to D^0(\to K^+K^-\pi^+\pi^-)K^-$ decays [12] are currently limited by our knowledge of the amplitude structure of $D^0 \to K^+K^-\pi^+\pi^-$ decays.

The LHCb Collaboration recently published a search for CPV through an amplitude analysis of $D^0 \to K^+K^-\pi^+\pi^-$ decays that employs the data collected during 2011

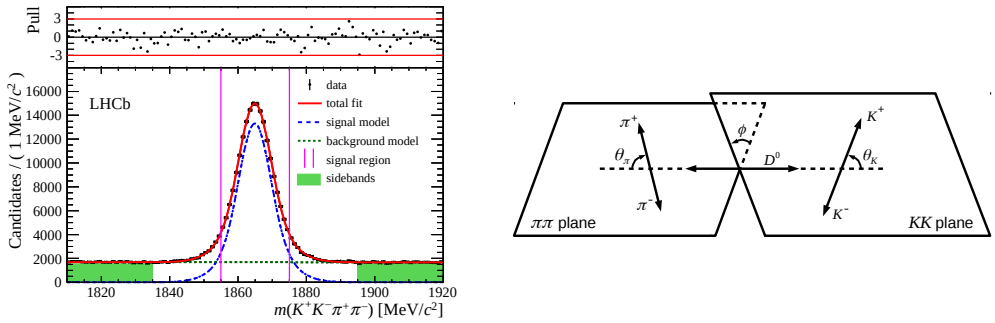

Fig. 3. – (Left) Mass distribution of the $D^0 \to K^+K^-\pi^+\pi^-$ candidates, with fit result superimposed. The top plot shows the normalised residuals. (Right) Definition of the helicity angles θ_K and θ_π, and of the decay-plane angle ϕ.

and 2012, corresponding to an integrated luminosity of $1(2)\,\text{fb}^{-1}$ of $p\ p$ collisions at $\sqrt{s} = 7(8)\,\text{TeV}$ [13]. The flavour at production of the D^0 meson is inferred from the sign of the muon charge in the decays $\overline{B} \to D^0\mu^-X$, where $\overline{B}$ is a b hadron and X represents an arbitrary set of unreconstructed particles. The trigger and the offline selection are optimised to maximise the purity, while keeping the efficiency as flat as possible across the final-state phase space. The $D^0 \to K^+K^-K^0_S$ decays are vetoed by removing all candidates that have a $\pi^+\pi^-$ invariant mass in the range $[480.2, 507.2]\,\text{MeV}/c^2$. The D^0-mass distribution after the selection is displayed in fig. 3 (left). About 160 thousand events with a purity of about 83% are obtained in the region within ± 2 standard deviations around the known D^0-meson mass [8]. This corresponds to about 50 times more signal candidates than those of the previous world-leading measurement, which used the data collected by the CLEO-c detector [14].

The five-dimensional phase space of the final state is parametrised using the Cabibbo–Maksymowicz variables [15]: the two invariant masses $m(K^+K^-)$ and $m(\pi^+\pi^-)$, the cosine of the helicity angles $\cos(\theta_K)$ and $\cos(\theta_\pi)$, defined as the angles between the direction of the D^0 momentum and that of one of the kaon (pion) mesons in the rest frame of the kaon (pion) mesons, and finally the angle ϕ between the planes defined by the directions of the two kaon mesons and the two pion mesons, respectively, in the D^0 rest frame. A visual representation of these three angles is given in fig. 3 (right). An unbinned maximum likelihood fit is performed, where the decay amplitudes are described with the isobar model [16, 17], which assumes that each amplitude can be built as a series of two-body decays. The four-body phase-space factor, the phase-space-dependent reconstruction efficiency and the background distribution are estimated with a large sample of simulated events and are included in the fit function. The amplitude model is determined by fitting the whole data sample, containing both D^0 candidates and $\overline{D}^0$ candidates, after a *CP* transformation is applied to the $\overline{D}^0$ daughters in the $\overline{D}^0$ rest frame. This allows to construct the signal model in a way that is blind to possible *CP*-violating effects. The results for the amplitudes pinpointed by the *CP*-averaged fit are listed in the first four columns of table I, where the fitted modulus and the phase of the complex coefficients c_k multiplying the amplitudes A_k of the isobar model are reported along with the fit fractions $\mathcal{F}_k$, defined as the branching ratios that would be observed if there was no interference among different decay amplitudes. The first four amplitudes account for more than 80% of the fit fractions. The fit projections for the five Cabibbo-Maksymowicz variables are displayed in fig. 4.

TABLE I. – *(Second to fourth column): Modulus and phase of the complex coefficients multiplying the decay amplitudes included in the CP-averaged fit model along with the corresponding fit fractions, $\mathcal{F}_k$. (Fifth to seventh column): Results for the CPV parameters fitted simultaneously to the D^0 and (CP-transformed) $\overline{D}^0$ samples, along with the asymmetries of the fit fractions. The first uncertainties are statistical and the second are systematic.*

Amplitude	$\lvert c_k\rvert$	$\arg(c_k)$ [rad]	$\mathcal{F}_k$ [%]	$A_{\lvert c_k\rvert}$ [%]	$\Delta\arg(c_k)$ [%]	$A_{\mathcal{F}_k}$ [%]
$D^0 \to [\phi(1020)(\rho-\omega)^0]_{L=0}$	1(fixed)	0(fixed)	$23.82 \pm 0.38 \pm 0.50$	0 (fixed)	0 (fixed)	$-1.8 \pm 1.5 \pm 0.2$
$D^0 \to K_1(1400)^+ K^-$	$0.614 \pm 0.011 \pm 0.031$	$1.05 \pm 0.02 \pm 0.05$	$19.08 \pm 0.60 \pm 1.46$	$-1.4 \pm 1.1 \pm 0.2$	$1.3 \pm 1.5 \pm 0.3$	$-4.5 \pm 2.1 \pm 0.3$
$D^0 \to [K^-\pi^+]_{L=0}[K^+\pi^-]_{L=0}$	$0.282 \pm 0.004 \pm 0.008$	$-0.60 \pm 0.02 \pm 0.10$	$18.46 \pm 0.35 \pm 0.94$	$1.9 \pm 1.1 \pm 0.3$	$-1.2 \pm 1.3 \pm 0.3$	$2.0 \pm 1.8 \pm 0.7$
$D^0 \to K_1(1270)^+ K^-$	$0.452 \pm 0.011 \pm 0.017$	$2.02 \pm 0.03 \pm 0.05$	$18.05 \pm 0.52 \pm 0.98$	$-0.4 \pm 1.0 \pm 0.2$	$-1.1 \pm 1.4 \pm 0.2$	$-2.6 \pm 1.7 \pm 0.2$
$D^0 \to [K^*(892)^0 \overline{K}^*(892)^0]_{L=0}$	$0.259 \pm 0.004 \pm 0.018$	$-0.27 \pm 0.02 \pm 0.03$	$9.18 \pm 0.21 \pm 0.28$	$-1.3 \pm 1.3 \pm 0.3$	$-1.7 \pm 1.5 \pm 0.2$	$-4.3 \pm 2.2 \pm 0.5$
$D^0 \to K^*(1680)^0[K^-\pi^+]_{L=0}$	$2.359 \pm 0.036 \pm 0.624$	$0.44 \pm 0.02 \pm 0.03$	$6.61 \pm 0.15 \pm 0.37$	$2.2 \pm 1.3 \pm 0.3$	$1.4 \pm 1.5 \pm 0.2$	$2.6 \pm 2.2 \pm 0.4$
$D^0 \to [K^*(892)^0 \overline{K}^*(892)^0]_{L=1}$	$0.249 \pm 0.005 \pm 0.017$	$1.22 \pm 0.02 \pm 0.03$	$4.90 \pm 0.16 \pm 0.18$	$-0.4 \pm 1.7 \pm 0.2$	$3.7 \pm 2.0 \pm 0.2$	$-2.6 \pm 3.2 \pm 0.3$
$D^0 \to K_1(1270)^- K^+$	$0.220 \pm 0.006 \pm 0.011$	$2.09 \pm 0.03 \pm 0.07$	$4.29 \pm 0.18 \pm 0.41$	$2.6 \pm 1.7 \pm 0.4$	$-0.1 \pm 2.1 \pm 0.3$	$3.3 \pm 3.5 \pm 0.5$
$D^0 \to [K^+K^-]_{L=0}[\pi^+\pi^-]_{L=0}$	$0.120 \pm 0.003 \pm 0.018$	$-2.49 \pm 0.03 \pm 0.16$	$3.14 \pm 0.17 \pm 0.72$	$3.5 \pm 2.5 \pm 1.5$	$-5.5 \pm 2.6 \pm 1.6$	$5.1 \pm 5.1 \pm 3.1$
$D^0 \to K_1(1400)^- K^+$	$0.236 \pm 0.008 \pm 0.018$	$0.04 \pm 0.04 \pm 0.09$	$2.82 \pm 0.19 \pm 0.39$	$0.2 \pm 2.9 \pm 0.7$	$2.5 \pm 3.5 \pm 1.0$	$-1.3 \pm 6.0 \pm 1.0$
$D^0 \to [K^*(1680)^0 \overline{K}^*(892)^0]_{L=0}$	$0.823 \pm 0.023 \pm 0.218$	$2.99 \pm 0.03 \pm 0.05$	$2.75 \pm 0.15 \pm 0.19$	$4.0 \pm 2.7 \pm 0.8$	$-5.4 \pm 2.8 \pm 0.8$	$6.2 \pm 5.2 \pm 1.5$
$D^0 \to [\overline{K}^*(1680)^0 K^*(892)^0]_{L=1}$	$1.009 \pm 0.022 \pm 0.276$	$-2.76 \pm 0.02 \pm 0.03$	$2.70 \pm 0.11 \pm 0.09$	$-0.4 \pm 2.1 \pm 0.3$	$0.4 \pm 2.1 \pm 0.3$	$-2.5 \pm 3.9 \pm 0.4$
$D^0 \to \overline{K}^*(1680)^0[K^+\pi^-]_{L=0}$	$1.379 \pm 0.029 \pm 0.373$	$1.06 \pm 0.02 \pm 0.03$	$2.41 \pm 0.09 \pm 0.27$	$2.1 \pm 2.0 \pm 0.6$	$-1.8 \pm 2.2 \pm 0.3$	$2.4 \pm 3.7 \pm 1.1$
$D^0 \to [\phi(1020)(\rho-\omega)^0]_{L=2}$	$1.311 \pm 0.031 \pm 0.018$	$0.54 \pm 0.02 \pm 0.02$	$2.29 \pm 0.08 \pm 0.08$	$0.8 \pm 1.9 \pm 0.3$	$-1.2 \pm 2.0 \pm 0.5$	$-0.1 \pm 3.3 \pm 0.5$
$D^0 \to [K^*(892)^0 \overline{K}^*(892)^0]_{L=2}$	$0.652 \pm 0.018 \pm 0.043$	$2.85 \pm 0.03 \pm 0.04$	$1.85 \pm 0.09 \pm 0.10$	$-0.6 \pm 2.5 \pm 0.4$	$0.6 \pm 2.6 \pm 0.4$	$-3.0 \pm 5.0 \pm 0.7$
$D^0 \to \phi(1020)[\pi^+\pi^-]_{L=0}$	$0.049 \pm 0.001 \pm 0.004$	$-1.71 \pm 0.04 \pm 0.37$	$1.49 \pm 0.09 \pm 0.33$	$3.8 \pm 3.1 \pm 0.7$	$-0.5 \pm 3.9 \pm 0.7$	$5.8 \pm 6.1 \pm 0.8$
$D^0 \to [K^*(1680)^0 \overline{K}^*(892)^0]_{L=1}$	$0.747 \pm 0.021 \pm 0.203$	$0.14 \pm 0.03 \pm 0.04$	$1.48 \pm 0.08 \pm 0.10$	$1.6 \pm 2.8 \pm 0.5$	$0.7 \pm 3.0 \pm 0.4$	$1.3 \pm 5.3 \pm 0.6$
$D^0 \to [\phi(1020)\rho(1450)^0]_{L=1}$	$0.762 \pm 0.035 \pm 0.068$	$1.17 \pm 0.04 \pm 0.04$	$0.98 \pm 0.09 \pm 0.05$	$4.6 \pm 4.1 \pm 0.6$	$9.3 \pm 3.3 \pm 0.6$	$7.5 \pm 8.5 \pm 1.1$
$D^0 \to a_0(980)^0 f_2(1270)^0$	$1.524 \pm 0.058 \pm 0.189$	$0.21 \pm 0.04 \pm 0.19$	$0.70 \pm 0.05 \pm 0.08$	$1.6 \pm 3.6 \pm 0.7$	$-7.3 \pm 3.3 \pm 0.8$	$1.5 \pm 7.2 \pm 1.3$
$D^0 \to a_1(1260)^+ \pi^-$	$0.189 \pm 0.011 \pm 0.042$	$-2.84 \pm 0.07 \pm 0.38$	$0.46 \pm 0.05 \pm 0.22$	$-4.4 \pm 5.6 \pm 3.7$	$9.3 \pm 6.1 \pm 1.3$	$-10.6 \pm 11.7 \pm 7.0$
$D^0 \to a_1(1260)^- \pi^+$	$0.188 \pm 0.014 \pm 0.031$	$0.18 \pm 0.06 \pm 0.43$	$0.45 \pm 0.06 \pm 0.16$	$-3.4 \pm 7.0 \pm 1.9$	$-5.8 \pm 5.6 \pm 4.3$	$-8.7 \pm 13.7 \pm 2.9$
$D^0 \to [\phi(1020)(\rho-\omega)^0]_{L=1}$	$0.160 \pm 0.011 \pm 0.005$	$0.28 \pm 0.07 \pm 0.03$	$0.43 \pm 0.05 \pm 0.03$	$2.1 \pm 5.2 \pm 0.8$	$-12.2 \pm 5.5 \pm 0.6$	$2.4 \pm 11.0 \pm 1.4$
$D^0 \to [K^*(1680)^0 \overline{K}^*(892)^0]_{L=2}$	$1.218 \pm 0.089 \pm 0.354$	$-2.44 \pm 0.08 \pm 0.15$	$0.33 \pm 0.05 \pm 0.06$	$5.2 \pm 7.1 \pm 1.9$	$-5.6 \pm 8.1 \pm 1.3$	$8.5 \pm 14.3 \pm 3.5$
$D^0 \to [K^+K^-]_{L=0}(\rho-\omega)^0$	$0.195 \pm 0.015 \pm 0.035$	$2.95 \pm 0.08 \pm 0.29$	$0.27 \pm 0.04 \pm 0.05$	$11.7 \pm 6.0 \pm 1.9$	$4.8 \pm 6.2 \pm 1.1$	$21.3 \pm 12.5 \pm 2.8$
$D^0 \to [\phi(1020) f_2(1270)^0]_{L=1}$	$1.388 \pm 0.095 \pm 0.257$	$1.71 \pm 0.06 \pm 0.37$	$0.18 \pm 0.02 \pm 0.07$	$2.7 \pm 6.7 \pm 1.7$	$0.9 \pm 6.0 \pm 1.7$	$3.6 \pm 13.3 \pm 3.0$
$D^0 \to [K^*(892)^0 \overline{K}_2^*(1430)^0]_{L=1}$	$1.530 \pm 0.086 \pm 0.131$	$2.01 \pm 0.07 \pm 0.09$	$0.18 \pm 0.02 \pm 0.02$	$3.9 \pm 5.2 \pm 1.0$	$6.8 \pm 6.4 \pm 1.4$	$6.1 \pm 10.8 \pm 1.8$
		Sum of fit fractions	$129.32 \pm 1.09 \pm 2.38$			
		χ^2/ndf	$9242/8121 = 1.14$			

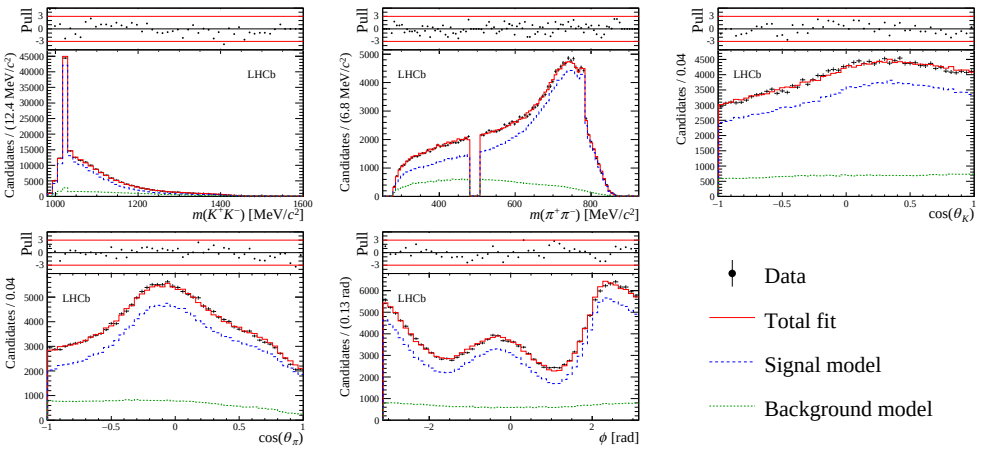

Fig. 4. – Distributions of the five Cabibbo–Maksymowicz variables for the selected D^0 and *CP*-transformed $\overline{D}^0$ candidates, with fit result superimposed. The plot on top of each distribution shows the normalised residuals, where the uncertainty is defined as the quadratic sum of the statistical uncertainties of the data and simulated samples.

Once the amplitude model is fixed, the fit is performed again, simultaneously for the D^0 and *CP*-transformed $\overline{D}^0$ samples, using as parameters the *CP*-averaged modulus and phase, the asymmetry of the moduli and the semidifference of the phases of the coefficients c_k of D^0 and *CP*-transformed $\overline{D}^0$ decays. The results, which are displayed in table I, are compatible with the hypothesis of *CP* conservation within an uncertainty that varies from 1% to 15%, depending on the amplitude. While the *CP*-averaged results are dominated by the systematic uncertainties due to the models used to describe the resonances and to the knowledge of their parameters, the precision of the *CPV* parameters is still statistically dominated. The results are the most precise to date for both the amplitude model and the search for *CPV* in $D^0 \to K^+K^-\pi^+\pi^-$ decays.

4. – Conclusions

Two recent searches of *CPV* in the decay of charm quarks by the LHCb Collaboration were reviewed in these proceedings. Both represent the best measurements of the respective observables to date and are consistent with the hypothesis of *CP*-symmetry conservation. The measurement described in sect. **2** will benefit soon from the addition to the data sample of the data collected by the LHCb experiment during 2018, corresponding to $2.1\,\text{fb}^{-1}$ of integrated luminosity of $p\,p$ collisions at $\sqrt{s} = 13\,\text{TeV}$, and by a detailed study of the shape of the radiative tails of the signal mass distributions, which is expected to reduce the dominant systematic uncertainty related to the assumed signal shapes in the fits to the mass distributions.

These results cover only a small part of the broad program of searches for *CPV* in charm decays at LHCb (further recent results are reviewed in ref. [18]). On one hand, a huge experimental effort is being pursued to measure *CPV* in the decay with precisions of the order of the SM expectations, 10^{-4} to 10^{-3}, for many D^0 and $D^+_{(s)}$ decay channels. This is fundamental since, owing to uncertainties introduced by nonperturbative QCD effects, it is unlikely that a single observation will be clearly interpretable as a SM effect or the manifestation of new interactions beyond the SM. However, the experimen-

tal values of the D-meson branching fractions allow to relate the expected size of *CPV* in different decay channels (see ref. [19] for a review of recent theoretical works in this direction). Therefore, new interactions beyond the SM might be identified from deviations of *CPV* from the predicted pattern in different decay channels. On the other hand, complementary searches look for time-dependent *CPV*, which allows for a stringent test of the SM since its expectations [20] still lie one order of magnitude below the current experimental sensitivity.

For both time-integrated and time-dependent measurements, the use of appropriate CF control modes and the choice of adequate analysis strategies ensure that all current LHCb results are still statistically limited despite the huge data samples analysed, often of order of 10^7 signal candidates [21]. The foreseen Upgrade I (2021–2029) [22] and the proposed Upgrade II (2031–2038) [23], which would increase the integrated luminosity collected by the LHCb experiment to $50\,\text{fb}^{-1}$ and $300\,\text{fb}^{-1}$ of $p\,p$ collisions at $\sqrt{s} = 14\,\text{TeV}$, respectively, will allow pushing the precision for both types of measurements below the 10^{-4} level. Together with the complementary work from the Belle II experiment—especially in final states including neutral particles [19]—, this will ensure a thorough test of the CKM mechanism in the sector of up-type quarks.

REFERENCES

[1] Cabibbo N., *Phys. Rev. Lett.*, **10** (1963) 531; Kobayashi M. and Maskawa T., *Prog. Theor. Phys.*, **49** (1973) 652.
[2] Dine M. and Kusenko A., *Rev. Mod. Phys.*, **76** (2003) 1.
[3] Grossman Y., Kagan A. L. and Nir Y., *Phys. Rev. D*, **75** (2007) 036008.
[4] LHCb Collaboration, *Nucl. Phys. B*, **871** (2013) 1; *JHEP*, **03** (2016) 159.
[5] LHCb Collaboration, *JINST*, **3** (2008) S08005; *Int. J. Mod. Phys. A*, **30** (2015) 1530022; *JINST*, **14** (2019) P04013.
[6] Benson S., Gligorov V. V., Vesterinen M. A. and Williams J. M., *J. Phys. Conf. Ser.*, **664** (2015) 082004.
[7] LHCb Collaboration, *Phys. Rev. Lett.*, **122** (2019) 191803.
[8] Particle Data Group, *Phys. Rev. D*, **98** (2018) 030001.
[9] LHCb Collaboration, *JHEP*, **07** (2014) 041.
[10] Yu F.-S., Wang D. and Li H.-N., *Phys. Rev. Lett.*, **119** (2017) 181802.
[11] Johnson N. L., *Biometrika*, **36** (1949) 149.
[12] Rademacker J. and Wilkinson G., *Phys. Lett. B*, **647** (2007) 400.
[13] LHCb Collaboration, *JHEP*, **02** (2019) 126.
[14] D'Argent P., Skidmore N., Benton J., Dalseno J., Gersabeck E., Harnew S., Naik P., Prouve C. and Rademacker J., *JHEP*, **05** (2017) 143.
[15] Cabibbo N. and Maksymowicz A., *Phys. Rev.*, **137** (1965) B438.
[16] Sternheimer R. M. and Lindenbaum S. J., *Phys. Rev.*, **123** (1961) 333.
[17] Herndon D., Soding P. and Cashmore R. J., *Phys. Rev. D*, **11** (1975) 3165.
[18] Jurik N. (on behalf of the LHCb Collaboration), this conference.
[19] Belle II Collaboration, BELLE2-PUB-PH-2018-001 (2018) pp. 415–429.
[20] Cerri A. *et al.*, CERN-LPCC-2018-06 (2018) pp. 57–61.
[21] LHCb Collaboration, *Phys. Rev. Lett.*, **116** (2016) 191601; *Phys. Lett. B*, **767** (2017) 177; *Phys. Rev. Lett.*, **118** (2017) 261803; *Phys. Rev. D.*, **97** (2019) 031101.
[22] LHCb Collaboration, CERN-LHCC-2012-007 (2012).
[23] LHCb Collaboration, CERN-LHCC-2017-003 (2017); CERN-LHCC-2018-027 (2018).